Materialwiss. Werkstofftech. **2019**, *50*, 1382–1390 **DOI** 10.1002/mawe.201800141

The effect of yttrium oxide in hydroxyapatite/aluminum oxide hybrid biocomposite materials: Phase, mechanical and morphological evaluation

Der Einfluss von Yttriumoxid in Hydroxylapatit/Aluminiumoxid hybriden Bioverbundwerkstoffen: Gefüge, mechanische und morphologische Evaluation

A. Özer[1], K.E. Öksüz[1]

This study presents the fabrication and characterization of composite materials of hydroxyapatite and aluminum oxide. Hydroxyapatite powder was obtained from bovine bones via conventional calcination routine. Although hydroxyapatite shows great biocompatibility with the human body, its applications are limited to non-load bearing areas. For this purpose, fine powders of hydroxyapatite/alumina were admixed with 1 and 5 wt.% yittria. Powder-compacts were sintered by two-step sintering route by increasing temperature to 1550 °C for 2 h and then sintering at 1450 °C for 4 h. The effect of increasing yittria content on sintering behavior and mechanical properties was investigated in biocomposite hybrid materials.

Keywords: Hydroxyapatite / yttria / composites / sintering / microstructure

Schlüsselwörter: Hydroxylapatit / Yttrium / Verbundwerkstoffe / Sintern / Gefüge

1 Introduction

Hydroxyapatite ($(Ca_{10}(PO_4)_6(OH)_2$, hereafter named as HA) has been widely used as a bone replacement material in restorative dental and orthopedic implants, due to its chemical and crystallographic structure being similar to that of bone mineral [1–2]. Extensive studies have indicated that hydroxyapatite is biocompatible with hard tissues of human beings and exhibits osteoconductive properties [3]. Thus, it is considered as the most promising bioactive material for clinical use [4–6]. However, despite its good biocompatibility and bioactivity, the low mechanical strength of hydroxyapatite restricts its applications for small and low load bearing implants and/or surface-coating of different implant materials [7–8]. Hence, the bulk use of hydroxyapatite requires an appropriate method for material to be toughened. Despite the many investigations and the important scientific findings on how to improve the mechanical properties of dense hydroxyapatite by modifying the processing parameters. But the improvements in mechanical characteristics of hydroxyapatite are not satisfactory, yet [9]. Eventually, the new trend in improving mechanical characteristics of hydroxyapatite has shifted to the development of this material in a composite form. The addition of a second mechanically resistant phase as reinforcement agent, such as a metal, ceramic increases the fracture toughness of hydroxyapatite ceramic matrix [9–10]. However, metals are not suitable as reinforcement agents due

[1] Sivas Cumhuriyet University, Department of Metallurgical and Materials Engineering, 58140, SİVAS, TURKEY

Corresponding author: K.E. Öksüz, Sivas Cumhuriyet University, Department of Metallurgical and Materials Engineering, 58140, SİVAS, TURKEY,
E-Mail: kerimemreoksuz@gmail.com

© 2019 WILEY-VCH Verlag GmbH & CO. KGaA, Weinheim

to the possible excessive corrosion reaction with hydroxyapatite, and undesirable reactions with tissues (increased levels of metal ions in implant tissues). The reinforcement of hydroxyapatite matrices with ceramic particles revealed to have considerable potential for improving the mechanical properties [11]. Among the many ceramics used in orthopedics, alumina is classified as a bioinert material with excellent friction and wear properties as well as minimal tissue reaction [12]. Therefore a composite system of the two components, the hydroxyapatite and the alumina, has potential as a synthetic biomaterial for hard tissues replacement because of its combined benefits: the osteoconductivity and bioactivity of hydroxyapatite and the excellent mechanical properties of alumina. There are several reports on hydroxyapatite/alumina composite, but very few on sintered yttria-doped hydroxyapatite/alumina composite. Effect of yttria content on the sintering behavior and mechanical properties of hydroxyapatite/alumina composites were not fully understood in the literature, yet.

In this study, an experimental attempt was made to improve the mechanical properties of hydroxyapatite via doping (1 and 5 wt.%) with yttria. Yttria has already been involved in biomedical applications, indirectly. In particular, yttria is well known since it is the most common stabilizer of zirconia [13]. Nowadays, stabilized zirconia enjoys wide clinical acceptance in dental and orthopedic applications, such as dental crowns and bridges, and femoral heads of hip implants, respectively [14–15]. Yttria stabilized zirconia has also been blended with hydroxyapatite and with various glasses in composite materials, or in plasma spray coatings [16–17]. Beyond zirconia, yttria-containing glass micro-spheres have been used very effectively for in situ radiotherapy of cancer [18].

2 Materials and experimental procedure

2.1 Production of hydroxyapatite

The powder of hydroxyapatite, namely BHA used in this study was derived from bovine bones. Bovine femoral bones were cut into small pieces and then they were rinsed with tap-water and soaked in a 1 wt.% concentration of antiseptic solution to prevent bad odor and contamination of various infectious diseases [19]. After washing and drying, the bone pieces were calcined at 850 °C with a heating rate of 5 °C min^{-1} and kept at that temperature for 4–5 h. in the air, as described elsewhere. [20]. Accordingly, the biologically derived hydroxyapatite powder used is very safe because they are produced via high temperature calcination method. Calcined bovine femoral bone parts were subjected to grinding with a blade grinder for 30 s. Following this resulting samples were then ball-milled until fine powder (i. e., with particles of submicron average size) of hydroxyapatite was obtained.

2.2 Preparation of bioceramic compositions

The powder of alumina (3–5 μm, $\rho = 3.99$ g/cm^3) and yttria (1–2 μm $\rho = 5.03$ g/cm^3) were purchased from Merck (Darmstadt, Germany). The hydroxyapatite-powder was mixed with 50 wt.% alumina fine powder. In this manner, matrix composition which will be used in the experimental study was prepared. 1 wt.% and 5 wt.% yttria were correspondingly mixed with hydroxyapatite and alumina powder and donated as BHAA, 1BHAA, 5BHAA respectively. The powder mixtures were well homogenized by ball milling in ethyl alcohol using a jar and balls made of zirconia (200 cycles/min, 24 h) with a ball to powder ratio of 20 : 1, *Figure 1*a–c. The batch suspensions were dried and the pellets with an approximate diameter of 13 mm and height of 10 mm were uniaxially pressed at 100 MPa in hardened steel dies, according to the British Standards (No. 7253) [21]. The green compact bodies were sintered at 1550 °C for 2 h and then 1450 °C for 4 h in static air in a closed alumina crucible and cooled to room temperature in the furnace. (The heating and cooling rates were 5 °C/min).

2.3 Characterization and mechanical properties

The following techniques were employed to characterize the produced sintered bioceramic materials. Micro-hardness tests were done with a Vickers micro-hardness testing equipment (Shimadzu micro-hardness tester type M, Japan; load of 1.961 N; the results were the average of ten different indentation measurements). Fracture toughness studies were

© 2019 WILEY-VCH Verlag GmbH & CO. KGaA, Weinheim

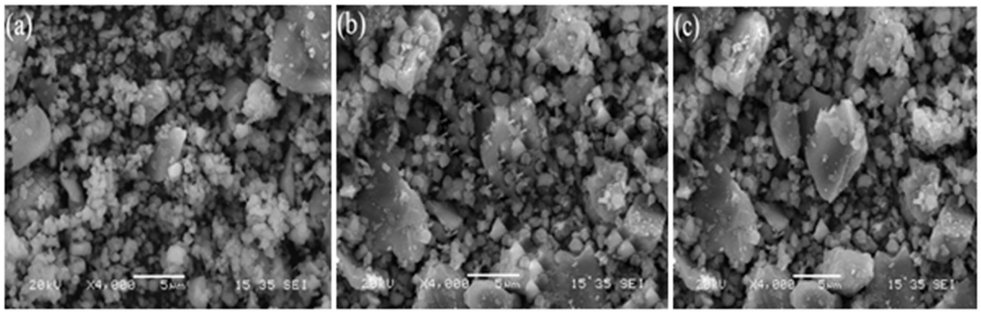


Figure 1. SEM image of initial powders after ball milling for 24 h. (a) BHAA, (b) 1BHAA (c) 5BHAA.

evaluated according to modified Griffith and Anstis theory of brittle materials. For this purpose, the micro hardness tests for fracture toughness were continued with 200 g for 30 s. and were measured under scanning electron microscope. This was aimed to propagate a crack origin at the corner of the notches of hardness measurements. The fractured crack was 3 times longer than the distance of d_1 and d_2 which lead to the formation of Palmqvist crack system. The Palmqvist crack system propagates from the corners with longer crack length than formed test area. The indentation fracture toughness was evaluated from Anstis with the following formula (Equation 1.) applied in previous studies [22–23].

$$K_{Ic} = 0.016 \left(\frac{E}{H}\right)^{1/2} x \frac{F}{c^{3/2}} \quad (1)$$

Where E is the elastic modulus of BHAA composites, H is the corresponding hardness, F is the applied load, and c is the crack length at each side.

The bulk density and the apparent porosity of the sintered specimens were measured using the Archimedes' principle. The vacuum method (ISO 10545-3) was used in the laboratory to determine the apparent porosity with greater precision. The vacuum method allows all open pores to be filled with water in this case and the vacuum process was conducted in a chamber in which the air pressure was lowered to a value of 10^{-3} mbar and held at that value for 30 minutes. Volume shrinkage (vol. %) was calculated through the samples' dimension measurements in pellet form using the same micro meter, before and after sintering. The microstructure of the samples (after thermal etching of polished surfaces) was observed by field emission scanning electron microscope (FE-SEM, Tescan $Mira_3$ XMU, Czechia). Composition analysis was performed using energy-dispersive spectroscopy apparatus attached to scanning electron microscope (EDS, INCA IE 350, and U.K.). A x-ray diffractometer (Rigaku D/MAX/2200/PC) with a monochromatic Cu–Kα radiation ($\lambda = 1.5408$ Å) was used over a 2θ range from 20° to 80° with a step size of 0.02 and a scan rate of 1°/minute to characterize the crystal structure of the sintered compacts, where the diffractograms were compared with the standards complied by the International Centre for Diffraction Data (ICDD).

3 Results and discussion

3.1 Physical and mechanical properties and densification

The experimental results of the densification and mechanical properties (micro-hardness and fracture toughness in this case) of the produced BHAA–yttria composites are recorded, *Figure 2*. In this study, the bulk densities of sintered pure BHAA were found as 3.268 g/cm^3 at 1550 °C 2 h and 1450 °C 4 h whereas the bulk densities of BHAA-yttria composites varied in the range of 3.27 g/cm^3–3.39 g/cm^3 depending on the yttria reinforcement amount. The increasing yttria amount increases the bulk density of the composites due to the higher crystal (theoretical) density of yttria. It was observed that the mechanical properties increase by high sintering temperature. Apparent porosity of sintered BHAA ceramic samples was found to be $1.32\,\% \pm 0.11$, $1.29\,\% \pm 0.13$ and $1.276\,\% \pm 0.09$ respectively. There is no significant change in ap-

© 2019 WILEY-VCH Verlag GmbH & CO. KGaA, Weinheim

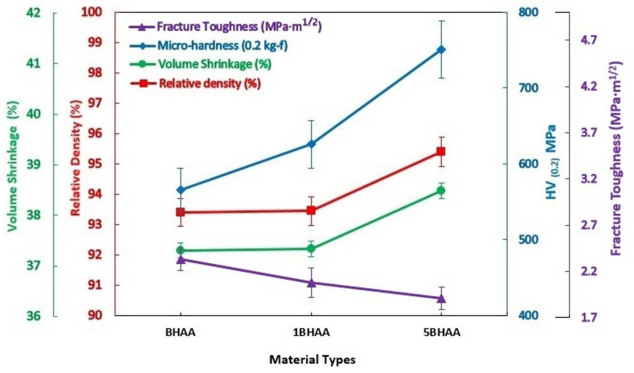


Figure 2. Variations in relative density, volume shrinkage, micro-hardness and fracture toughness in HA/Al_2O_3 composites with different Y_2O_3 contents.

parent porosity (%) in sintered ceramic samples which are around 1.29 % ± 0.5 %. The impact of yttria in BHAA matrix was pronounced by microhardness values. The obtained values are also considerably higher than that of the BHAA matrix samples. These high hardness values may be concluded to the increasing glassy phase and/or yttria amount. To the best of our knowledge, this is the first time that 5 wt.% yittria is reported to a certain mix composition of 50 wt.% hydroxyapatite – 50 wt.% alumina.

The increasing glassy phase by the yttrium addition at two step sintering temperature may lead to increased density and hardness while a slight decrease in fracture toughness can be concluded to the increased glass content in ceramics. The compositional fluctuations and heterogeneities in ceramic microstructure may occur and cause a decrease in toughness values. Also the formation of calcia-yttria-phosphate related phases accompanying to calcium-phosphate and calcia-alumina phases can affect the toughness values which are crack sensitive and propagates the crack with higher energy due to the increased atomically heterogeneous structure, Figure 2. The decreased fracture toughness values are acceptable in all ranges due to higher density over 95 % even for calcium-phosphate. The yttria addition leads to increase in hardness due to higher density while a slight decrease in fracture toughness values within the 30 % range. It decreases from 2.31 MPa·m(1/2) to 1.89 MPa·m(1/2) which is about a regular ceramic structure as glass or alumina of 95 % dense. A slight decrease in shrinkage values may be explained with the addition of yttria. By yttria addition, the increasing glassy phase formation and binary/ternary phase diagram relations between calcia-alumina-yttria can be derived due to higher densification characteristics at the same sintering regime. Since the densification increased slightly by increasing yttria content, the shrinkage is obvious to follow the same trend.

3.2 Phase evaluation

The x-ray diffraction patterns of the bioceramic composites sintered as described above are summarized, *Figure 3*. Four crystalline phases, namely hibonite – ($CaO(Al_2O_3)_6$), beta-tricalcium phosphate – ($Ca_3(PO_4)_2$), calcium yttrium phosphate – $Ca_9Y(PO_4)_7$ and aluminium yttrium oxide – ($AlYO_3$) with varying peak intensities, could be detected in patterns by increasing yttria content. In all cases, the diffractograms have predominantly registered the phase of hibonite – ($CaO(Al_2O_3)_6$, matched for every sample (ICSD card no. 76-0665). X-ray diffraction patterns of hydroxyapatite/alumina composite powders show that the peaks correspond to hydroxyapatite and alumina phases, confirming that alumina is effectively incorporated into the hydroxyapatite matrix. The figure proves that the hydroxyapatite/alumina composites are successfully produced without noticeable undesirable phases. The X-ray diffraction reflections at 34.2° and 35.9° 2θ degrees are corresponding to hibonite (hexagonal dihexagonal dipyramidal). The main peaks of beta-tricalcium phosphate are also visible at 31.1° and 34.3° 2θ° where one of the main peak of hibonite was overlapped by beta-tricalcium phosphate and the peak became asymmetric. The x-ray diffraction pattern indicates that both phases can coexist due to the hydroxyapatite/alumina interaction for the bioceramic and its composites as can be described by equation (2) followed by equation (3), while equation (4), equation (5) and equation (6) describe the possible formation of yttria related phases. Figure 3a, b, c. The higher mass loss observed for hydroxyapatite at ~1150 °C is related to the water release produced by the transformation of hydroxyapatite to beta-tricalcium phosphate according to the reaction equation (2) [24–25].

© 2019 WILEY-VCH Verlag GmbH & CO. KGaA, Weinheim

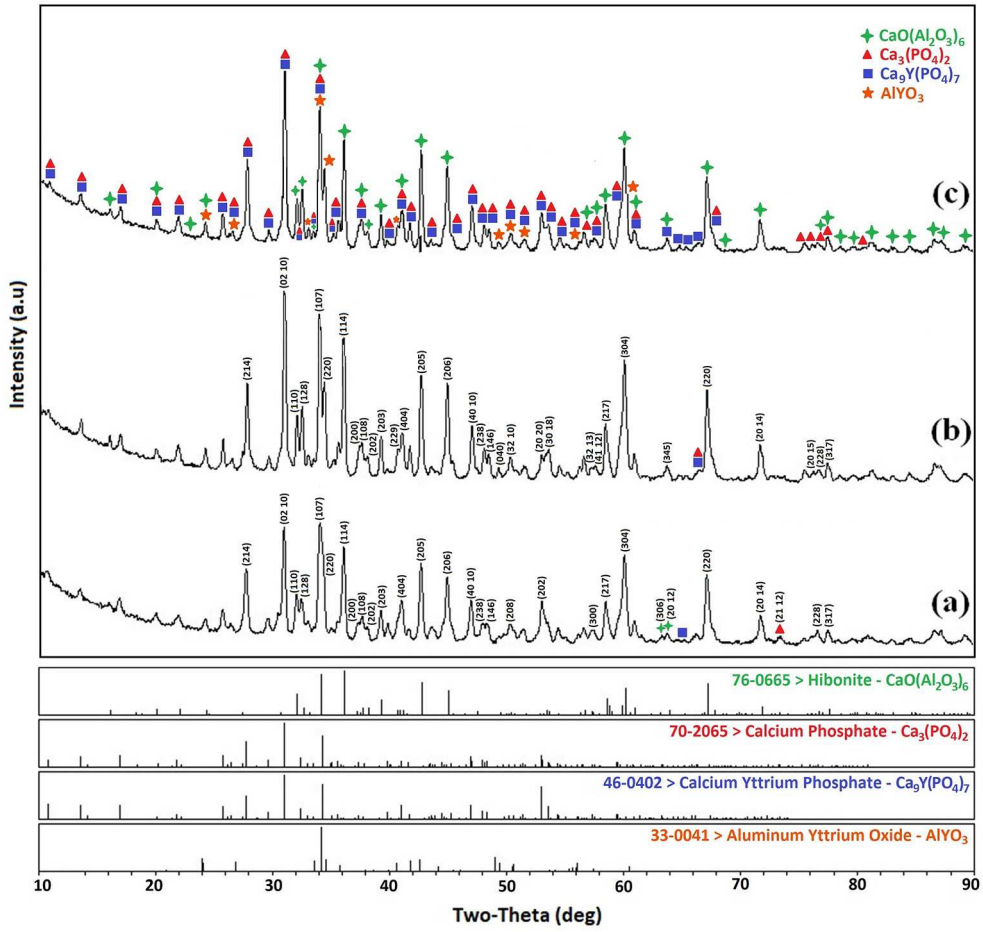


Figure 3. XRD patterns of biocomposite samples obtained with various amounts of Y_2O_3 after two-step sintering. (a) BHAA, (b) 1BHAA, (c) 5BHAA.

$$Ca_{10}(PO_4)_6(OH)_2 \rightarrow 3Ca_3(PO_4)_2 + CaO + (H_2O)\ \uparrow \quad (2)$$

$$CaO + 6Al_2O_3 \rightarrow CaO(Al_2O_3)_6 \quad (3)$$

$$Y_2O_3 + Ca_3(PO_4)_2 = 2YPO_4 + 3CaO \quad (4)$$

$$16YPO_4 + 9Ca_{10}(PO_4)_6(OH)_2 = 3Y_2O_3 + 10Ca_9Y(PO_4)_7 + 9H_2O \quad (5)$$

$$Y_2O_3 + Al_2O_3 = 2AlYO_3 \quad (6)$$

As clarified in literature, the dehydroxylation and rehydratation reactions were occurred under a critical point of 1300 °C [26–27]. Beyond this temperature the reactions are irreversible anymore while cooling. It has been mostly reported that hydroxyapatite can partially decompose into tricalcium phosphate and calcium oxide at this sintering temperature. The effects of various amounts of yttria on the phase transition of hydroxyapatite/alumina-yttria sintered biocomposites are shown in x-ray diffraction patterns, Figure 3b, c. X-ray diffraction patterns also demonstrates that the peak intensities of BHAA composite are lower than that of the 1BHAA and 5BHAA composites, revealing that the addition of yttria promotes the crystallization of hydroxyapatite. The yttria could not be detected in the x-ray diffraction patterns after sintering as a pure substance, suggesting that Y^{3+} ions diffuse into the hydroxyapatite lattice and occupied the interstitial positions, as expected, because of the size difference of their ionic radii [28]. Increasing the yttria content from 1 wt.% yttria to 5 wt.% yttria for samples 1BHAA and 5BHAA sintered in two step cycle as at 1550 °C 2 h and 1450 °C 4 h. favored the formation of calcium yttrium phosphate (ICSD card

© 2019 WILEY-VCH Verlag GmbH & CO. KGaA, Weinheim

no. 33-0041) and aluminium yttrium oxide (ICSD card no. 46-0402) peak was doubled as expected, Figure 3b, c. In order to investigate the difference between BHAA and 1BHAA, 5BHAA biocomposite samples were compared and it was clearly seen that calcium yttrium phosphate formation ($2\theta = 49°$, 64°) was favored in the latter and significant existence of diffraction peaks belonging to calcium yttrium phosphate was observed for 1BHAA biocomposite at $2\theta = 31.4°$, 41°, 47.2°, 53°, Figure 3a, b. This behavior was also observed for 5BHAA biocomposite. When the diffraction graphs of 5BHAA samples sintered with the same cycle were examined, aluminium yttrium oxide phase was evaluated as a new phase due to the possibility of a reaction between alumina and yttria by increasing yttria content. X-ray diffraction pattern suggest the presence of aluminium yttrium oxide phase (which are significantly distinguished at $2\theta = 24.1°$ (increases the existing peak), 34.2°, 41.8°, 49°), Figure 3c. This phase is also evident with the formation of other smaller peaks related to the aluminium yttrium oxide, Figure 3c. Increasing yttria content, even at same sintering temperature may increase the glassy phase formation as indicated in diffraction patterns due to the possible eutectic reactions among calcium oxide-aluminum oxide-yttrium oxide. It's known that calcium oxide-aluminum oxide binary phase diagram has a eutectic around 1400 °C and Al_2O_3-Y_2O_3 binary phase diagram has a eutectic at 1850 °C that means calcium oxide-aluminum oxide-yttrium oxide should have a eutectic under 1400 °C.

3.3 Microstructure and morphological evaluation

The surface morphology of the BHAA biocomposites was examined by scanning electron microscopy, equipped with an energy dispersive spectrometer. The samples were fixed on aluminium stubs and pre-coated with gold/palladium thin film for 5 min under argon atmosphere using a Technics Hummer II sputter coater. The scanning electron microscopy samples were examined at an accelerating voltage of 20 kV. Energy dispersive spectra was used to determine their surface composition with $\approx 1\,\mu m^2$ resolution and source energy of 10 keV. Three runs were repeated and averaged for the surface elemental analysis of each specimen.

Scanning electron microscopy images of sintered biocomposites were presented after polishing and thermal etching of the sample surfaces, *Figure 4*a–f. Scanning electron microscopy images reveal that homogenous morphology and different grain size distribution were obtained for all compositions after sintering. Images indicate that sintering occurred at sintering cycle that applied to samples which can be characterized by the formation of significant amounts of glassy phase, whereas the developed microstructure featured an obvious evidence of high densification, Figure 4b, d, f.

Scanning electron microscopy images also represents the surface morphology of samples become smoother by increasing yttria content due to increasing glassy phase, Figure 4a, c, e. As observed, especially in scanning electron microscopy image, the increasing glassy phase and yttria may contribute to the smoothness of the surface and more particles seem to be embedded to the matrix structure, Figure 4b, d, f. Some smaller particles are remark-

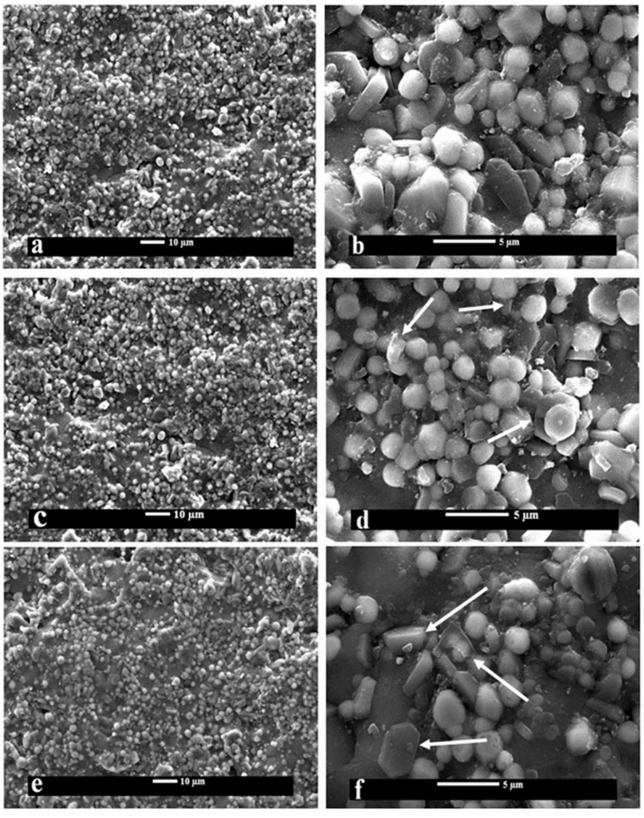


Figure 4. SEM images of the two-step sintered BHAA-Y_2O_3 biocomposites. (a)–(b)BHAA, (c)–(d) 1BHAA (d)–(e) 5BHAA. (White arrows show the liquid/solid phase single crystal growth characteristics).

© 2019 WILEY-VCH Verlag GmbH & CO. KGaA, Weinheim

able in scanning electron microscopy images due to having liquid/solid phase single crystal growth characteristics as shown by white arrows, Figure 4d, f.

Average grain sizes of the samples were calculated from the microstructure of the surface. At least 50 grains were averaged for each image. The average grain sizes of the sintered biocomposite ceramics were calculated to be around ~2.75 µm, ~2.05 µm and ~2.03 µm, respectively, Figure 4b, d, f. By increasing yttria addition, it is found that the average grain size has a slight decrease.

Sinterization is the most important step in manufacturing a ceramic body with high physical properties of interest. It determines, in large part, the final properties of the ceramic, such as microstructure, mechanical properties and final crystalline phases and in the case of bioceramics, their behavior in service. Temperature, time, initial particle size of the material, sintering atmosphere, nature of additives, etc. are important factors which can influence the sintering process and the resulting microstructure. The sintering, which has a heat-assisted treatment nature by atomic diffusion mechanisms usually improves the mechanical strength of the material (in this case) through the formation of a solid bond between the particles. This process is generally accompanied with densification (i.e. elimination of the pores) and strengthening of the compact, a process driven by interfacial energy (γ) [28–29]. To choose two step sintering cycle drive the sintering both in high temperature (at 1550 °C 2 h) to increase the grain boundary areas for more atomic diffusion and low temperature (at 1450 °C 4 h) to promote the higher diffusion for densification but not for an abnormal grain growth. The sintering at higher temperature shouldn't be proceeded to cause grain growth due to high diffusion rate.

The neck formation and growth between contiguous particles results in a solid bonded network polycrystalline microstructure with the pores entrapped, *Figure 5*a. When the biocomposite samples were exposed to sintering, the residual pores become smaller in size and number, and isolated from each other to be eliminated in further process, Figure 5b. The mechanical properties of the composite are associated with the bonding strength between the component phases. Therefore, a chemical reaction at the matrix-reinforcement interface could mechanically increase the interfacial bond in spite

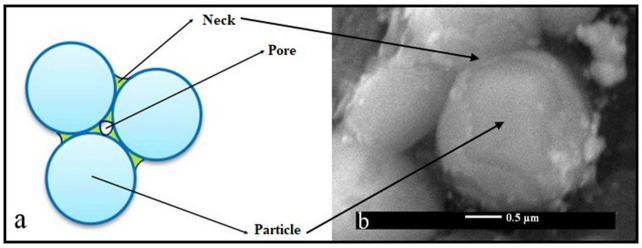


Figure 5. (a) Schematical representation of sintering model geometry of spherical particles. (b) SEM microstructure of a two-step sintered HA/Al_2O_3-5 wt.% Y_2O_3 compact.

of the new phase formation. Experimental data are strongly supporting the idea of existence of a very good wetting between hydroxyapatite-alumina particles and yttria reinforcement.

Energy dispersive x-ray spectroscopy was involved to explore the morphology and elemental composition of the biocomposite samples after sintering. Elemental analysis results were obtained by the aerial elemental analysis for each sample surface, *Figure 6*a–f. Energy dispersive x-ray spectroscopy results show a calcium/phosphate ratio close to stoichiometric ratios for hydroxyapatite, which is around 1.55–1.67 in literature and x-ray diffraction graphs confirm that hibonite and beta-tricalcium phosphate, are the stable phases at room temperature after sintering [28]. The energy peaks corresponding to calcium, phosphorus and aluminum elements from energy dispersive x-ray spectroscopy analysis are very strong for all compositions while the yttria element can be detected for 1BHAA and 5BHAA biocomposites by increasing yttria addition, Figure 6d, f. Results in energy dispersive x-ray spectroscopy also indicate that the precipitate formed on the surface of the composite is a beta-tricalcium phosphate, hibonite containing, calcium, aluminum and phosphorus-rich phase, which coincides with the x-ray diffraction results.

4 Conclusions and future works

- Powders of hydroxyapatite (derived from bovine bone)/alumina composites with varying concentrations of the yttria were produced using a conventional powder metallurgy route and successfully sintered by two-step cycle.
- The main phases of the sintered bioceramic composites were hibonite, beta-tricalcium phosphate,

© 2019 WILEY-VCH Verlag GmbH & CO. KGaA, Weinheim

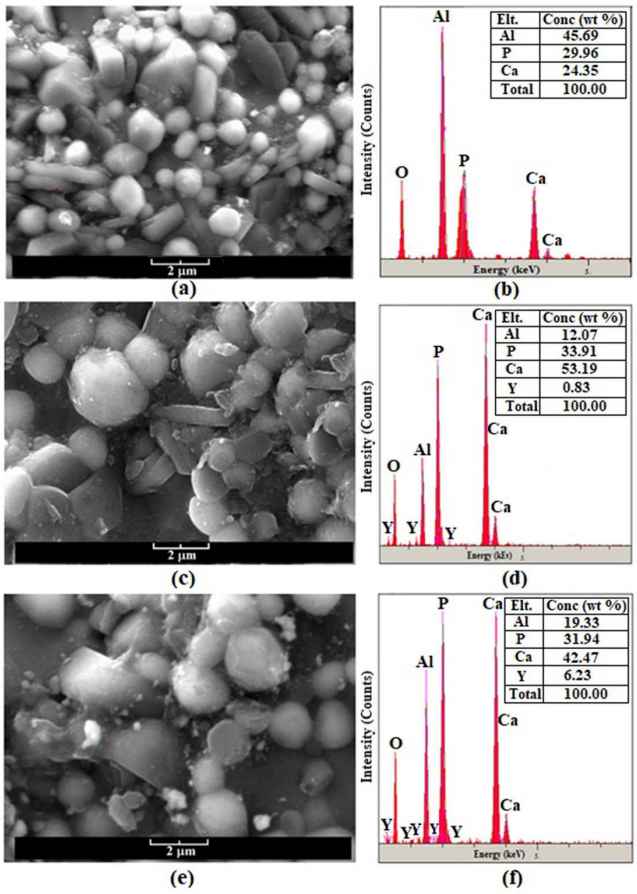


Figure 6. (a)–(c)–(e) SEM images of the two-step sintered BHAA,1BHAA,5BHAA biocomposites respectively. (b)–(d)–(f) The EDX spectra of the two-step sintered surfaces of BHAA, 1BHAA,5BHAA biocomposites, respectively.

calcium yttrium phosphate and aluminium yttrium oxide depending on the yttria content which are known biocompatible.

- The addition of yttria favors the glassy phase formation in biocomposite samples, encouraging the grain boundary migration, and consequently closing the open pore structure by high diffusion rate.
- Yttria may promote the crystallization of hydroxyapatite within a multi component phase matrix.
- Doping of hydroxyapatite/alumina with oxides are seemingly a promising way for improving its mechanical properties. Consequently, natural BHA may be a reliable, promising, safe and low-cost source for easily producing hydroxyapatite/alumina - yttria biocomposites.
- The reproducible microhardness, fracture toughness, phase analyses and morphological evaluation suggest that these materials would have good performance in load bearing applications. The produced bulk structure in this work can be either in pulverized or in bulk form.
- The obtained material may be suitable to be used as a graft material for tooth and bone substitute and deficiency after *in vitro* and *in vivo* tests. This procedure was implied to be as a very near future work.

5 References

[1] W. Wang, K.W.K. Yeung, *Bioact Mater.* **2017**, *2*, 224.
[2] V. Campana, G. Milano, E. Pagano, M. Barba, C. Cicione, G. Salonna, W. Lattanzi, G. Logroscino, *J. Mater. Sci. Mater. Med.* **2014**, *25*, 2445.
[3] S.M. Zakaria, S.H. Sharif Zein, M.R. Othman, F. Yang, J.A. Jansen, *Tissue Eng. Part B Rev.* **2013**, *9*, 431.
[4] K.E. Öksüz, A. Özer, *Acta. Phys. Pol. A.* **2017**, *131*, 576.
[5] M. Mahmoodi, P.M. Hashemi, R. Imani, *Prog Biomater.* **2014**, *3*, 25.
[6] J. Torres, M. Gutierres, L. Atayde, P. Cortez, M.A. Lopes, J.D. Santos, A.T. Cabral, C.F. Van, *J. Orthop. Res.* **2017**, *35*, 1176.
[7] Y.M. Kong, C.J. Bae, S.H. Lee, H.W Kim, H. E Kim, *Biomaterials* **2005**, *26*, 509.
[8] B. Bulut, Z.E. Erkmen, E.S. Kayali, *J. Ceram. Sci. Tech.* **2016**, *7*, 263.
[9] H.A. Siddiqui, K.L Pickering, M.R. Mucalo, *Materials* **2018**, *11*, 1813.
[10] Li. Feng, J. Xiaosong, S. Zhenyi, Z. Degui, Z. Luo, *Nanomaterials* **2018**, *8*, 729.
[11] X. Zhao, J. Yang, H. Xin, X. Wang, L. Zhang, F. He, Q. Liu, W. Zhang, *Mater. Sci. Eng. C.* **2018**, *91*, 135.
[12] M. Hafid, *Bioceram. Dev. Appl.* **2017**, *1*, 98.
[13] S. Nath, N. Sinha, B. Basu, *Ceram. Int.* **2008**, *34*, 1509.
[14] L. Gremillard, S. Tadier, *Advances in Ceramic Biomaterials*, Woodhead Publication, France **2017**.
[15] S. Sequeira, M.H. Fernandes, N. Neves, M.M. Almeida, *Ceram. Int.* **2017**, *43*, 693.
[16] W. Yu, X. Wang, J. Zhao, Q. Tang, M. Wang, X. Ning, *Ceram. Int.* **2015**, *41*, 10600.

© 2019 WILEY-VCH Verlag GmbH & CO. KGaA, Weinheim

[17] O. Gunduz, Z. Ahmad, S. Salman, A.T. Inan, N. Ekren, S. Agathopoulos, L.S. Özyeğin, E. S. Kayali, F.N. Oktar, *Adv. Mater. Res.* **2012**, *445*, 982.
[18] M.R. Ghahramani, A.A. Garibov, T.N. Agayev, M.A. Mohammadi, *Glass. Phys. Chem.* **2014**, *40*, 283.
[19] A. Niakana, S. Rameshan, P. Ganesana, C.Y. Tana, J. Purbolaksonoa, Hari Chandranb, S. Rameshc, W.D. Teng, *Ceram. Int.* **2015**, *41*, 3024.
[20] K.E. Öksüz, A. Özer, *Dig. J. Nanomater. Biostruct.* **2016**, *11*, 167.
[21] British Standard Non-metallic materials for surgical implants. Part 2. Specification for ceramic materials based on alumina, BS (No 7253), ISO 6474–1981, **1990**.
[22] L. Ćurković, V. Rede, K. Grilec, A. Mulabdić, presented at *MATRIB'07*, Vela Luka, Crotia, June 21–23, **2007**, pp. 40–45.
[23] A. Nastica, A. Merati, M. Bielawski, M. Bolduc, O. Fakolujo, M. Nganbe, *J. Mater. Sci. & Techn.* **2015**, *31*, 773.
[24] S.F. Ou, S. Chiou, K.L. Ou, *Ceram. Int.* **2013**, *39*, 3809.
[25] S.J. Lee, Ji-Yeon Kwak, W.M. Kriven, *J. Ceram. Process. Res.* **2012**, *13*, 243.
[26] B.M. Isaacson, L.B. Brunker, A.A. Brown, J. P. Beck, G.L. Burns, R.D. Bloebaum, *J. Biomed. Mater. Res. Part B: Appl. Biomater.* **2011**, *97*, 190.
[27] M. Prakasam, J. Locs, K. Salma-Ancane, D. Loca, A. Largeteau, L. Berzina-Cimdina, *J. Funct. Biomater.* **2015**, *6*, 1099.
[28] C. Vasconcelos, Sintering of Ceramics – New Emerging Techniques, Intechopen Press, Portugal **2012**.
[29] A. Özer, W.M. Kriven, Y.K. Tür, *Mater. Sci. and Eng. A* **2012**, *556*, 878.

Received in final form: December 27th 2018

© 2019 WILEY-VCH Verlag GmbH & CO. KGaA, Weinheim